ELSEVIER

Journal of Atmospheric and Solar-Terrestrial Physics 70 (2008) 1034–1045

Journal of ATMOSPHERIC AND SOLAR-TERRESTRIAL PHYSICS

www.elsevier.com/locate/jastp

Effects of geomagnetic storm on GPS ionospheric scintillations at Sanya

Guozhu Li[a,*], Baiqi Ning[a], Biqiang Zhao[a], Libo Liu[a], J.Y. Liu[b], K. Yumoto[c]

[a]*Institute of Geology and Geophysics, Chinese Academy of Sciences, Beijing 100029, China*
[b]*Institute of Space Science, National Central University, Chung-Li, Taiwan*
[c]*Space Environment Research Center, Kyushu University, Japan*

Received 18 April 2007; received in revised form 27 November 2007; accepted 1 January 2008
Available online 17 January 2008

Abstract

The effects of geomagnetic storm on GPS ionospheric scintillations are studied here using GPS scintillation data recorded at Sanya (18.3°N, 109.5°E; geomagnetic: 7.6°N, 180.8°E), the southmost station in the Chinese longitude region. GPS scintillation/TEC and DMSP data are utilized to show the development of irregularities during the period year 2005 (solar minimum). Statistical analysis of *K* planetary index (Kp) and amplitude scintillation index (S4) indicates that most storms of the year did not trigger the scintillation occurrence at Sanya. However, cases of scintillation occurring during moderate and strong storm ($Dst < -100$) periods show clearly that the development of irregularities producing scintillations can be triggered by geomagnetic storms during the low scintillation occurrence season. The effects (trigger or not trigger/inhibit) depend on the maximum dDst/dt determined local time sector, and can be explained by the response of the equatorial vertical drift velocities to magnetospheric and ionospheric disturbance electric fields. For station Sanya, the maximum dDst/dt determined local time is near the noon (or post-midnight) sector for most storms of the year 2005, which inhibited (or did not trigger) the post-sunset (or post-midnight) scintillation occurrence and then led to the phenomena that the statistical results presented.

Keywords: Equatorial ionosphere; Ionospheric scintillations; Irregularities; Electric fields

1. Introduction

Plasma irregularities in the nighttime equatorial F region, namely as equatorial spread-F (ESF) (Woodman and La Hoz, 1976), have been the subject of many observational and theoretical investigations over the past several decades (e.g. Fejer and Kelley, 1980; Kelley, 1989; Fejer, 1996; Fejer et al., 1999). These irregularities are formed in the post-sunset period due to the Rayleigh–Taylor gravitational instability processes operating on the steep upward gradient in the bottomside F-region. They produce amplitude and phase scintillations on trans-ionospheric satellite signals from VHF to L band mainly near the geomagnetic equator. The strongest L band scintillations, with signal fades of about 20 dB, often occur during solar maximum years, in the equatorial anomaly regions during the

*Corresponding author. Tel.: +86 10 62007712; fax: +86 10 62010846.
E-mail address: GZLee@mail.iggcas.ac.cn (G. Li).

1364-6826/$ - see front matter © 2008 Elsevier Ltd. All rights reserved.
doi:10.1016/j.jastp.2008.01.003

post-sunset period (Aarons, 1982; Basu et al., 1988). With the increasing reliance on satellite-based positioning systems in critical applications, the impact of scintillation on GPS communications has generated a new impetus. Since scintillation prediction can help to avoid blackouts and distortions in GPS communications due to ionospheric irregularities, it also can help to advance the understanding of the nature of scintillations. The prediction of the scintillation during geomagnetic storms, and how geomagnetic storms affect the occurrence of scintillation, as one of the prominent issues related to space weather studies, is very important for radio communications.

Previous studies of the effects of geomagnetic storms on ESF and equatorial plasma bubbles (EPBs) have shown that there is a general consensus that geomagnetic activity tends to suppress the generation of ESF in the pre-midnight period, whereas the possibility of observing ESF during the post-midnight period increases with geomagnetic activity. Aarons and DasGupta (1984) studied the major magnetic storm of April 1981, using the scintillation data from two equatorial stations. They found that the probability of occurrence of post-midnight equatorial scintillation activity is enhanced if the recovery phase of the storm starts in the midnight to dawn local time sector. Dabas et al. (1989), considering the scintillation data from a chain of stations extending from the equator to 21°N magnetic latitude along 84°E in the Indian zone and at Lunping in the far eastern zone, reported the local time effects on scintillation activity during different phases of geomagnetic storms. By analyzing the equatorial scintillation data during the magnetic storms based on Kp and Dst indices, Aarons (1991) concluded that the ring current can play a leading role directly or indirectly in establishing the conditions for equatorial F-layer irregularity generation or inhibition, and categorized Dst variations during magnetic storms on categories when maximum Dst occurs: (1) 10:00–16:00 LT, (2) 00:00–06:00 LT and (3) 18:00–22:00 LT, and found that the first category of storms had more suitable conditions for the inhibition of scintillation. Now the category is known as "Aarons criteria" (Biktash, 2004). Recently, Basu et al. (2001) related the occurrence of strong irregularities with the change rates of Dst lower than −50 nT/h. By considering a less stringent criterion, Huang et al. (2002) concluded that the rates of change lower than −5 nT/h for 2 or more hours would trigger equatorial irregularities, likely due to the penetration of high-latitude electric fields.

During periods of geomagnetic storms, the equatorial electric fields could be affected by two main high-latitude sources, namely the solar wind–magnetosphere dynamo (direct or prompt penetration of the magnetospheric convection electric field) and the ionospheric disturbance dynamo. The equatorial zonal electric field affects the growth rate of the Rayleigh–Taylor instability through the gravitational and electrodynamic drift terms and by controlling the electron density gradient in the bottomside of the F layer after dusk. Therefore, the equatorial post-sunset electric field should play a dominant role in the variability of ESF (Farley et al., 1970). Kelley and Maruyama (1992) presented case studies of storm-time electric field effects on the generation of ESF over Jicamarca during post-midnight hours and tested the assumption that the penetration of eastward plasmaspheric electric fields initiates the generation of these irregularities. However, Fejer (1996) presented that prompt penetration electric fields alone cannot explain the complex dependence of ESF on magnetic activity. In addition, Fejer et al. (1999) explained the dependence of spread-F occurrence on magnetic activity as due mostly to the corresponding variability of the equatorial vertical plasma drifts, and reported a threshold level of ~50 m/s (~20 m/s) $\mathbf{E}\times\mathbf{B}$ drift velocity at solar maximum (solar minimum).

Recently, the GPS ionospheric scintillations at a low-middle latitude station Wuhan in China during storms were studied (Li et al., 2006; Xu et al., 2006, 2007). In the present study, GPS scintillation/TEC measurements at Sanya (18.3°N, 109.5°E), Digisonde and DMSP plasma density data from other longitude sectors are utilized to study the effects of geomagnetic storms on equatorial ionospheric scintillations during the low scintillation occurrence season (for station Sanya, the GPS ionospheric scintillations mainly occur during equinoctial months (3, 4, 9, 10), and are rarely observed at solstice). We continue the investigations in which source can have an influence on scintillation activity, and the main objective of the study is to find out which source can be related to the scintillation occurrence during storm periods in the Chinese sector. IMF Bz, Dst and dDst/dt are used to identify the geomagnetic storms. The net horizontal magnetic field intensity ΔH ($H_{\text{equator}}-H_{\text{non-equator}}$, nT), introduced by Chandra and

Rastogi (1974), together with the virtual height of the F layer h′F, the variations of $\mathbf{E}\times\mathbf{B}$ drift velocity are illustrated. In general, observational results show that scintillation development can be triggered or inhibited (not triggered) during geomagnetic storms. The maximum dDst/dt determined time is nearly the same as penetration time estimated by ΔH, and it determined that local time plays a main role in the development of irregularities.

2. Data

In order to understand the amplitude and phase scintillation of GPS L1 band in the Chinese low-latitude region, a modified GPS receiver was set up at Sanya (18.3°N, 109.5°E). The receiver is a NovAtel Euro4 dual-frequency receiver version with OEM4 card and special firmware, which also yields the value of ionospheric TEC (Van Dierendonck et al., 1993). The amplitude scintillation is monitored by computing the S4 index, which is the standard deviation of the received power normalized by its mean value. For the cases presented in this paper, only the signals coming from satellites with an elevation angle higher than 15° and with a time of lock longer than 180 s were taken into account.

The plasma data used here are from the observations of Special Sensor—Ions, Electrons, and Scintillation (SSIES) package onboard the DMSP satellite. The DMSP satellites are three-axis stabilized spacecraft that fly in Sun-synchronous circular polar orbits at ~840 km altitude. The orbital planes are near either the 18:00–06:00 or 21:00–09:00 geographic LT meridians with the ascending nodes on the duskside of the earth. SSIES consists of a spherical Langmuir probe mounted on a 0.8 m boom to measure the densities and temperatures of ambient electrons, along with three separate sensors mounted on a conducting plate facing in the ram direction (Rich and Hairston, 1994). The data we used in this study are from the DMSP F15 satellite (the orbit is in the sector 21:00 LT) and the time resolution of used data is 4 s, which can be used to investigate the post-sunset EPB occurrence at a wide longitude region.

By adopting the technique of Chandra and Rastogi (1974), the daily variations of vertical $\mathbf{E}\times\mathbf{B}$ drift velocity were observed with the ΔH (nT) parameter at ~110°E longitude. H is the horizontal intensity of the geomagnetic field. If the variations of H away from the equator ($H_{\text{non-equator}}$) are removed, the non-ionospheric variations can be eliminated from the H_{equator} data. Thus the ΔH parameter ($H_{\text{equator}}-\mathrm{H}_{\text{non-equator}}$) is a good indicator of the vertical $\mathbf{E}\times\mathbf{B}$ drifts velocity. Here, the equatorial Muntinlupa (14.4°N, 121.0°E; geomagnetic: 3.6°N, 191.6°E) and non-equatorial Sanya (18.3°N, 109.5°E; geomagnetic: 7.6°N, 180.8°E) magnetometer data were used to obtain the ΔH parameter and infer the $\mathbf{E}\times\mathbf{B}$ drift due to prompt penetration. The virtual height of F layer, h′F, and the peak height of F layer, hmF2, are measured by Digisonde at Chungli (CL, 24.9°N, 121.2°E). Together, the measurements h′F at Kwajalein (KJ, 8.7°N, 167.7°E) are utilized to estimate the vertical drift velocity. The Kwajalein Digisonde data are obtained from the DIDB database.

Geomagnetic storms are characterized by a prolonged depression of the horizontal component (H) of the Earth's magnetic field. The depression in H is characterized by the geomagnetic index Dst, obtained from the Space Physics Interactive Data Resource. The southward turning of the interplanetary magnetic field (IMF) Bz ensures the transportation of solar wind energy into the Earth's magnetosphere, which is the primary cause for the formation of geomagnetic storms (Allen et al., 1989; Tsurutani et al., 1992; etc). Here, IMF Bz, Dst and dDst/dt indices are used to classify the storms. IMF Bz and Kp data are obtained from Coordinated Data Analysis Web.

3. Results

3.1. Statistical analysis of geomagnetic activity (Kp) and scintillation occurrence (S4)

The correlation between geomagnetic activity based on Kp index and occurrence of scintillation has been investigated. As shown in Fig. 1, the 3-h Kp values are plotted versus the amplitude scintillation index (S4) observed at Sanya during the year 2005. From the figure we can see that the scintillation occurrence is mainly confined to periods of lower Kp values, and for periods with higher Kp values ($\mathrm{Kp}>4+$), there are nearly no scintillation occurrences. The results indicate that scintillation may easily occur during geomagnetic quiet days at Sanya, and geomagnetic disturbance may not trigger the scintillation occurrence. Since ionospheric irregularities producing scintillation were generated a few hours after the beginning of the disturbance, in order to make the correlation

between Kp and scintillation occurrence more realistic, here, the used Kp value is the maximum Kp value for the previous and current 3 h.

3.2. Storm cases

3.2.1. Storm 1: 8 May 2005

Here we present a case that the irregularities producing scintillations at Sanya were triggered by a geomagnetic storm. The enhancements of vertical upward drifts due to the storm helped to create the right conditions for irregularities to develop, and then induced the scintillations.

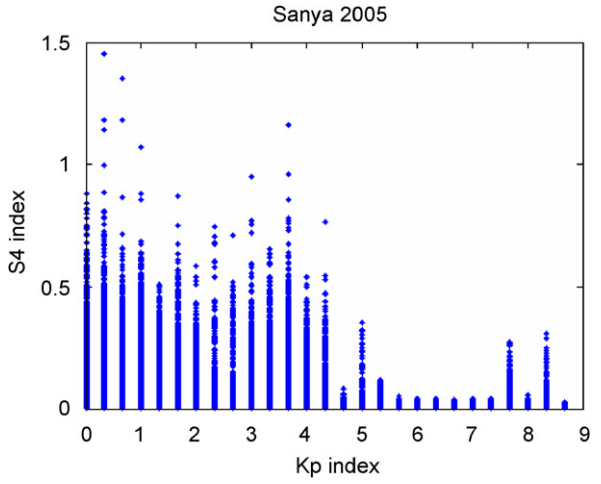

Fig. 1. Three-hour Kp index versus amplitude scintillation index (S4) observed at Sanya during the period year 2005.

In Fig. 2, the three left panels show the IMF Bz, Dst and rate of change of Dst (dDst/dt). ΔH parameter, the virtual height of F layer h′F and peak height of F layer hmF2 are presented in the three right panels. As shown in the top left panel, IMF Bz turned southward at around 18:00 UT on 7 May 2005 and reached the maximum value ~ -19 nT. Except for several northward excursions, it remained negative for several hours until 07:30 UT on 8 May 2005. And then, IMF Bz again turned southward at around 11:50 UT. In the middle panel, Dst index showed two maximum negative excursions -91 and -127 nT at about 03:00 and 18:00 UT. However, the maximum dDst/dt -36 and -27 nT appeared at 01:00 and 12:00 UT. The top right panel shows two sudden increases in ΔH near 01:00 and 12:00 UT on 8 May; this behavior is most likely associated with the effect due to the prompt penetration of an eastward electric field into the equatorial ionosphere. Low-latitude Digisonde station Chungli (CL) registered a very significant increase of the F layer.

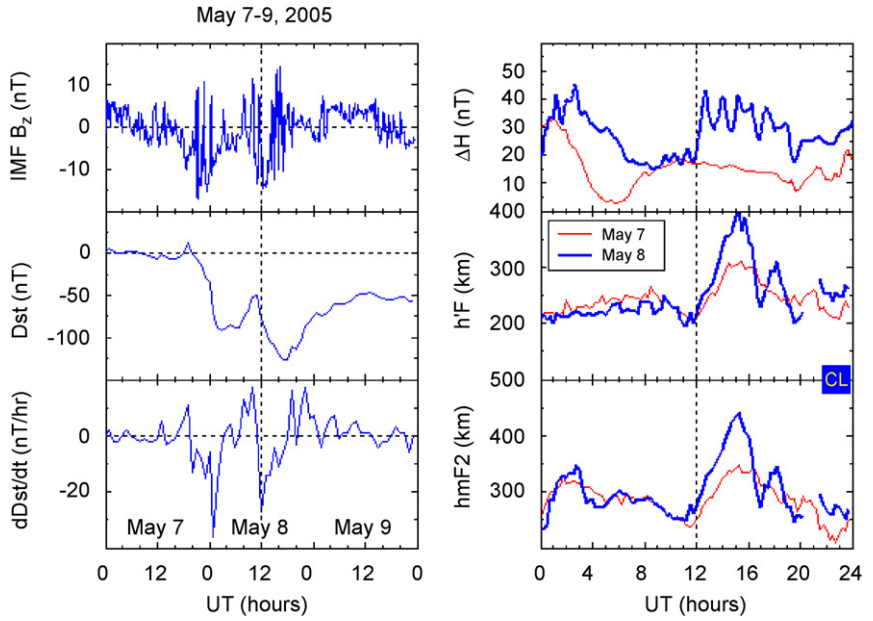

Fig. 2. Bz component of the interplanetary magnetic field in geocentric–solar–magnetospheric (GSM) coordinates provided by the Advanced Composition Explorer (ACE) spacecraft (top panel, left), Dst index (middle panel, left), the rate of change of Dst index (bottom panel, left) for the period 7–9 May 2005; ΔH parameter (top panel, right) for 7–8 May 2005; F layer virtual height (h′F, middle panel, right) and F layer peak height (hmF2, bottom panel, right) obtained from Digisonde measurements at CL (Chungli) for 7–8 May 2005.

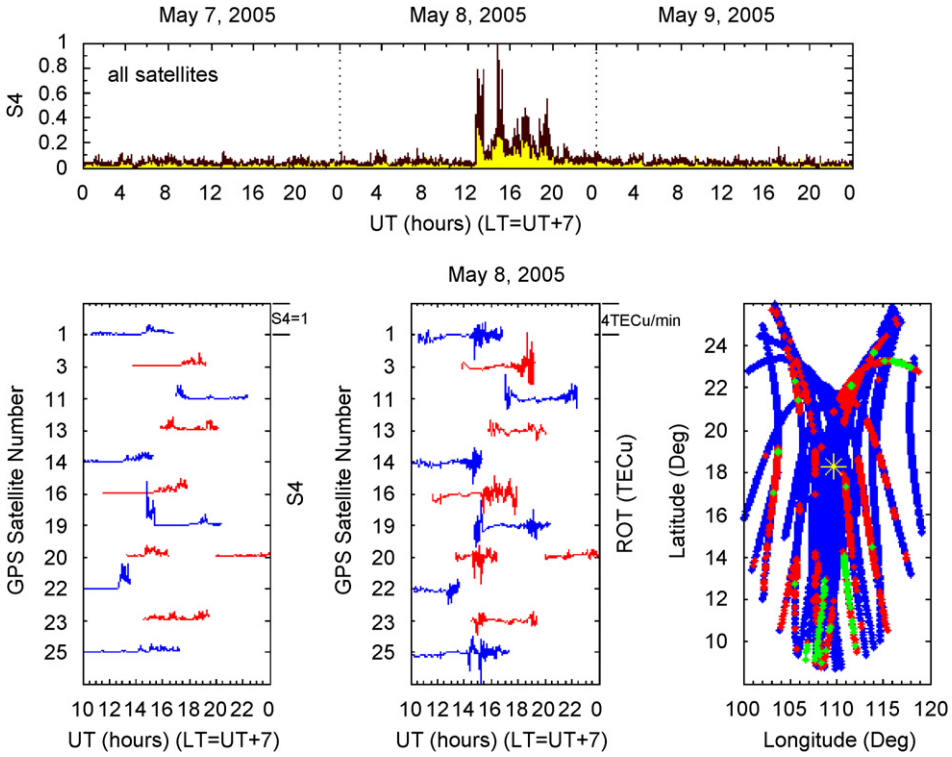

Fig. 3. GPS amplitude scintillations (S4 index) for all satellites during the period 7–9 May 2005(top panel), and scintillations and TEC fluctuations (ROT) on 8 May 2005 at Sanya (bottom panels). Vertical axes of bottom left and middle panels represent satellite number. Separation between satellites is 1 (for S4 index) and 4 TECu/min (for ROT). The bottom right panel is a map of GPS satellite tracks in the 400 km altitude from Sanya (marked by asterisk), red and green bold traces represent the weak ($0.3 > S4 \geqslant 0.1$) and moderate ($S4 \geqslant 0.3$) scintillations, respectively.

As seen from the two bottom right panels of Fig. 2, both h′F and hmF2 showed a sudden increase, which started at 12:00 UT, and related the enhancement of the vertical upward $\mathbf{E} \times \mathbf{B}$ drift velocity. h′F went gradually from 225 km at 12:00 UT to 405 km at 15:15 UT during 8 May, and the average upward plasma drift velocities are estimated about ~15 m/s. In the evening sector, when the upward drifts are larger than ~5–10 m/s near the solar minimum, narrow unstable layers of weak irregularities will be generated in the lower F region in all seasons. For upward drift velocities larger than ~15–20 m/s, the unstable layer is lifted to altitudes where the gravitational drift term is dominant in the growth rate of the Rayleigh–Taylor instability, leading to wide and strong scattering regions (Fejer et al., 1999).

The GPS scintillations and TEC fluctuations recorded at Sanya are shown in Fig. 3. The top panel shows the amplitude scintillations for all satellites during the period 7–9 May 2005. Only on the night of 8 May there exist apparent scintillations. The bottom left panel shows that scintillations are observed from many GPS satellites and the scintillation is very strong, and S4 index is more than 1 for PRN 19. The bottom middle panel of Fig. 3 shows the UT variation of ROT (rate of change of TEC per minute, Pi et al., 1997), a measure of the presence of ionospheric irregularities. For PRN 19, the maximum ROT is more than 4 TECu. From these two panels, we can clearly see that the observed scintillation started at post-sunset 13:00 UT (~20:00 LT) and continued to post-midnight after 19:00 UT (~02:00 LT). The bottom right panel of Fig. 3 shows that the scintillations occurred at a wide region around station Sanya.

For the storm, the above-presented figures indicate that the magnetospheric perturbations influence the equatorial ionosphere, and lead to the post-sunset steep height increase of h′F, which causes the Rayleigh–Taylor mode to become unstable, and results in spread-F irregularities. Hence, strong scintillations and TEC fluctuations were observed at Sanya during ~13:00–19:00 UT.

If we use the maximum dDst/dt as the category, for station Sanya (LT ≈ UT + 7), the maximum dDst/dt (12:00 UT) determined local time is about 19:00 LT, which corresponds to the post-sunset sector.

3.2.2. Storm 2: 24 August 2005

In contrast with storm 1, the storm of 24 August 2005 as indicated in Figs. 4 and 5 showed that little GPS scintillation was observed at Sanya, but TEC fluctuation was apparent and the EPBs were observed by DMSP F15 at the ~147°E longitude region during the storm period. Figs. 4 and 5 show IMF Bz, Dst, dDst/dt, ΔH, h′F and hmF2 indices, and S4, ROT and plasma density (Ni), respectively.

As shown in Fig. 4, IMF Bz exhibited two incursions to the south on 24 August 2005. The first one turned southward and reached the maximum value ~−55 nT at around 09:00 UT, and then turned northward at 10:40 UT. After approximately 30 min, IMF Bz again became southward at 11:08 UT and remained negative until 12:20 UT. The maximum Dst index found was −216 nT at 11:00 UT. However, the rate of change of Dst (dDst/dt) reached a maximum −158 nT/h at 10:00 UT. Also, the ΔH parameter showed a sudden increase nearly within the period 10:00–11:00 UT. h′F and hmF2 showed several increments during 09:00–11:00, 11:00–13:00 and 13:00–15:00 UT.

The GPS scintillations and TEC fluctuations recorded at Sanya are shown in Fig. 5. The top panel shows the amplitude scintillations for all satellites during the period 23–25 August 2005. Only on the night of 24 August did there exist a little scintillation. As the bottom left panel presented, the scintillation was observed only by PRN 16 and PRN 20, and the maximum S4 index was about 0.4. The bottom middle panel of Fig. 5 shows the UT variation of ROT. Different from little scintillation, the TEC fluctuation was observed by many satellites, and the maximum fluctuation reached 4 TECu. It indicates that for most PRN passes there exist large-scale irregularities (shown as apparent TEC fluctuations), but no small-scale irregularities (Fresnel scale) producing GPS ionospheric scintillations (e.g. Basu et al., 1999).

Data from the DMSP satellite (F15) can be processed to obtain the occurrence of EPBs in other longitude regions. Ma and Maruyama (2006) utilized the ion density to identify a super storm-time bubble. As shown in the right bottom panel of Fig. 5, it indicates that the DMSP F15 crossed three structures, centered near 147°E at 10:48 UT, in which the plasma density decreased rapidly from 10^5 to 10^3 cm^{-3}. For station Sanya and the 147°E longitude region, the maximum dDst/dt (10:00 UT) determined local time is ~17:00 and ~20:00 LT, respectively.

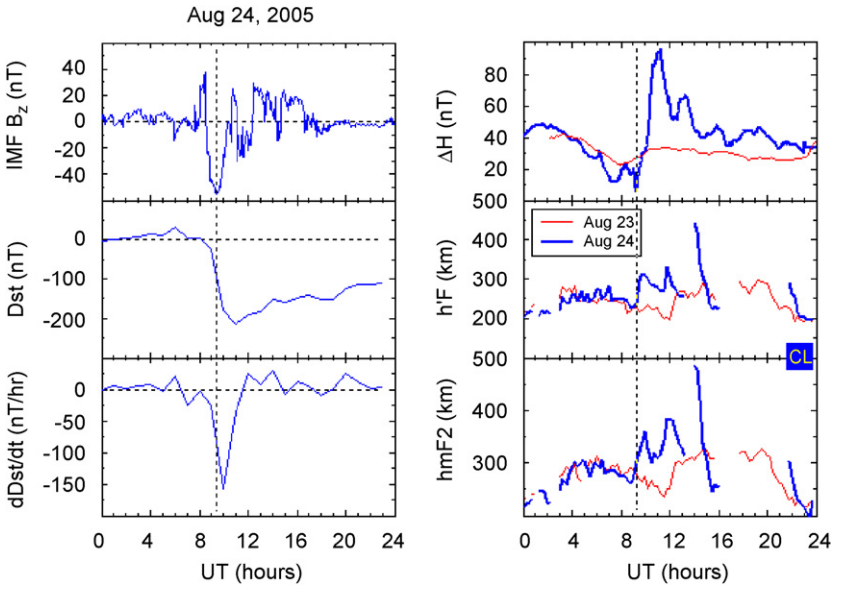

Fig. 4. Same as Fig. 2; Bz component of IMF, Dst index, rate of change of Dst index for 24 August 2005; ΔH parameter, h′F and hmF2 for 23–24 August 2005.

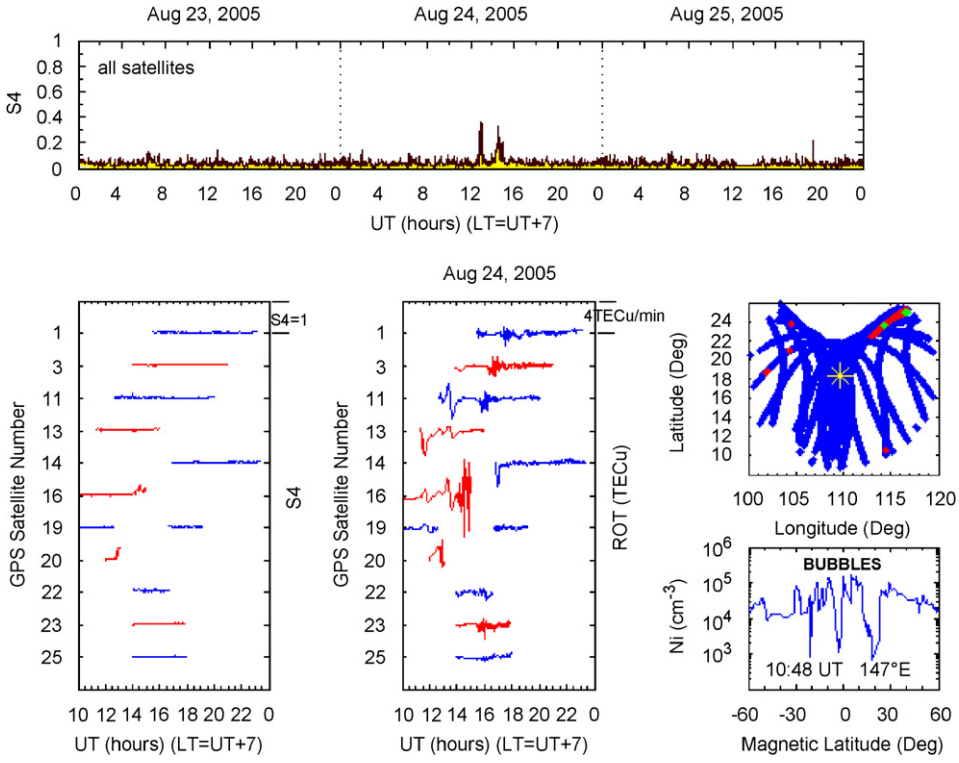

Fig. 5. GPS amplitude scintillations (S4 index) for all satellites during the period 23–25 August 2005(top panel). The two bottom left panels show S4 index and ROT obtained from Sanya for 24 August 2005. Separation between satellites is 1 (for S4 index) and 4 TECu/min (for ROT). The right middle panel is a map of GPS satellite tracks. The right bottom panel shows the plasma density measurements from DMSP F15 on 24 August 2005 at longitude ~147°E (~10:48 UT).

3.2.3. Storm 3: 15 May 2005 and other storms

In comparison to scintillation activity during storms 1 and 2, no scintillation and TEC fluctuation were observed at Sanya during the storms that occurred on 21 January, 15 May, 30 May, 12 June and 11 September 2005. However, the EPBs were observed by DMSP F15 or strong spread-F was recorded at other longitude regions during the storm periods (near the maximum dDst/dt determined time). Here, the storm of 15 May 2005 is presented in detail. Figs. 6 and 7 show IMF Bz, Dst, dDst/dt, ΔH, h′F (for CL and KJ) and hmF2 (for CL and KJ) indices, and S4, ROT, plasma density (Ni) and plasma vertical drift velocity (Vz), respectively.

Fig. 6 illustrates that IMF Bz turned southward at 05:30 UT on 15 May 2005 and then turned northward at 08:25 UT. The maximum IMF Bz component is over −46 nT. As seen from the two left middle panels, Dst and dDst/dt reached their maximum −263 nT and −170 nT/h at 08:00 and 07:00 UT, respectively. The ΔH parameter showed a sudden increase nearly at 07:00 UT. The four right panels show measurements of h′F and hmF2 for Chungli and Kwajalein. For station Kwajalein, h′F and hmF2 registered a very significant increase during the period ~06:20–07:40 UT, followed by the occurrence of strong spread-F (seen as diffuse F-region traces in the ionogram). By using the h′F (KJ) increment ~177 km, the average upward plasma drift velocities are estimated about 37 m/s during the period 06:20–07:40 UT. As previously introduced, this drift velocity is larger than ~15–20 m/s, and the unstable layer will be lifted to altitudes where the Rayleigh–Taylor mode becomes unstable, and then the spread-F will be generated and cause the scintillations.

Fig. 7 shows the GPS scintillation and TEC fluctuation recorded at Sanya, and the topside plasma density and vertical drift velocity measurements at the 191°E longitude sector. As seen from the top panel, GPS amplitude scintillation was observed by PRN 3 on 14 May 2005. On the following two nights, there was no observed scintillation activity. The bottom left and middle panels show the detailed information about scintillation

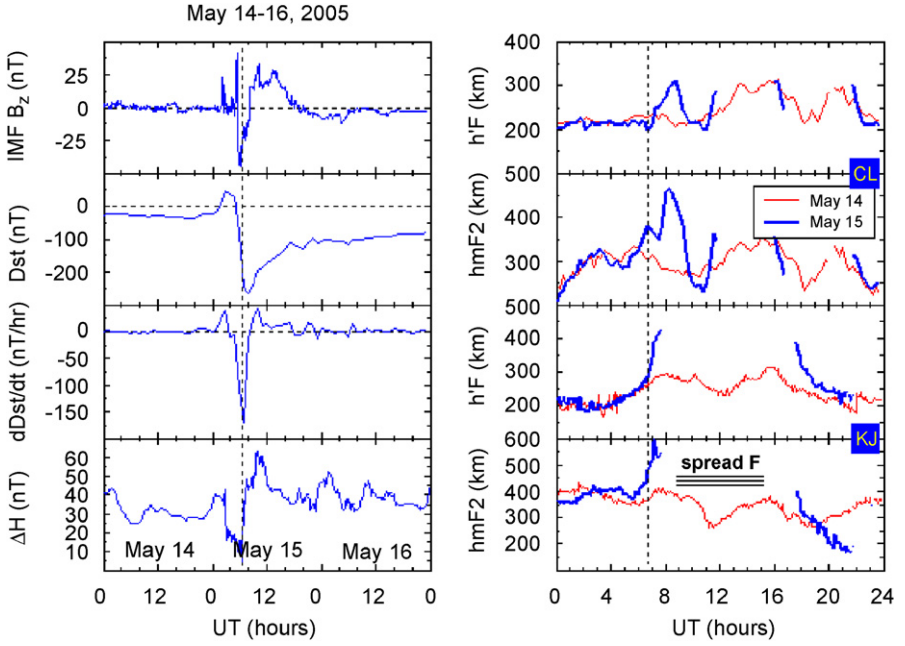

Fig. 6. Same as Fig. 2; Bz component of IMF, Dst index, rate of change of Dst index and ΔH parameter for the period 14–16 May 2005; h′F and hmF2 (CL and KJ) for 14–15 May 2005.

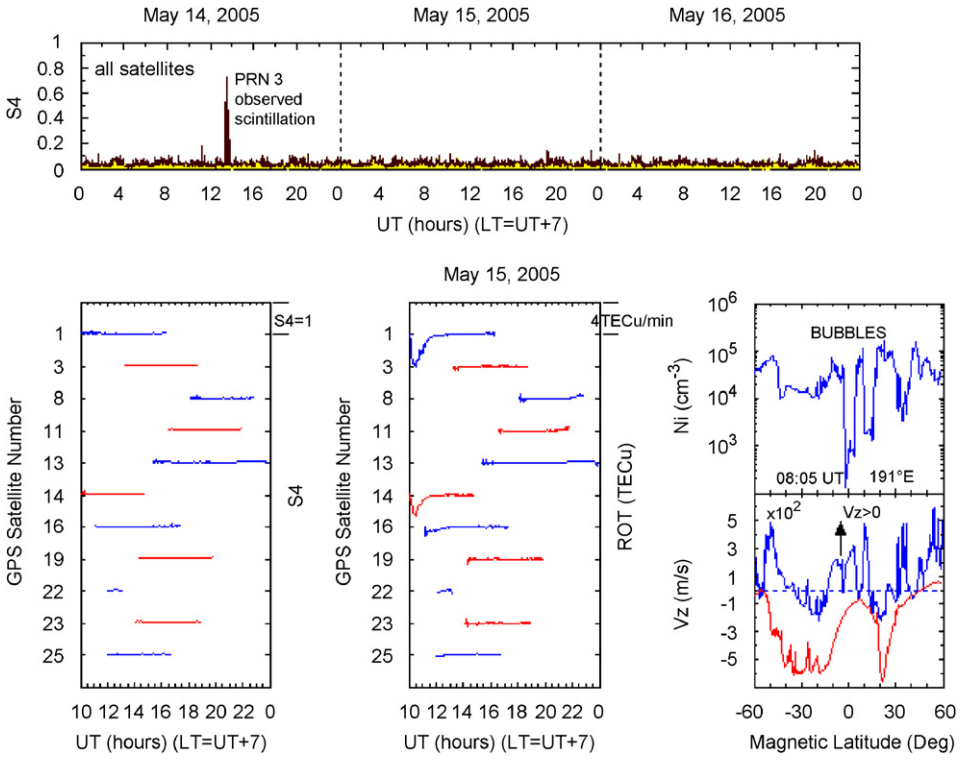

Fig. 7. GPS amplitude scintillations (S4 index) for all satellites during the period 14–16 May 2005(top panel). Two left panels show S4 index and ROT obtained from Sanya for 15 May 2005. Separation between satellites is 1 (for S4 index) and 4 TECu/min (for ROT). The right middle and bottom panels show the plasma densities and the plasma vertical flow velocities (red line indicates the velocity during the same period for the previous day) from DMSP F15 passes on 15 May 2005 at longitude ~191°E (~08:05 UT).

and TEC fluctuation during the storm period. Although no scintillation and TEC fluctuation was observed at Sanya, the occurrence of EPBs was detected by DMSP F15 in other longitude regions. As shown in the right middle and two bottom panels, the deep plasma depletions were located near 191°E at ~08:05 UT. Within the depletions, the plasma density decreased from 10^5 to $10^2\,cm^{-3}$. Also, the simultaneous topside plasma drift velocity Vz showed upward drifts. For station Sanya, Kwajalein and the 191°E longitude region, the maximum dDst/dt (07:00 UT) determined local time is ~14:00, ~18:00 and ~20:00 LT, respectively.

4. Discussion

The cases presented here indicate that there can be different effects (trigger or inhibit/not trigger) of storm on GPS ionospheric scintillations at Sanya. The maximum dDst/dt determined local time played a dominant role in the development of irregularities, and at the time close to the post-sunset sector, the storm will help to create the right conditions for post-sunset irregularities.

In the equatorial region, one of the necessary conditions for the generation of F-region irregularities is that the F-layer should be lifted to a higher region, where the Rayleigh–Taylor mode becomes unstable, and then form plasma bubbles and spread-F irregularities. The F-layer height is largely determined by the equatorial vertical drift velocity, which is driven by the zonal electric field via the $\mathbf{E} \times \mathbf{B}$ drift. Through analyzing a large database of equatorial F region plasma drift velocities derived from Jicamarca radar observations, Fejer and Scherliess (1997) and Scherliess and Fejer (1997) modeled the storm-time behavior of the equatorial electric fields and delineated the contributions from prompt penetration and disturbance dynamo electric fields. Generally, nighttime (daytime) F-layer drifts are normally downward (upward) because of the westward (eastward) electric field. Before the reversal of the drift from upward to downward, there exists an upward drift enhancement named prereversal enhancement. A clear relation exists between the magnitude of the prereversal enhancement and occurrence of post-sunset ESF: when a strong prereversal enhancement presents, the irregularities are more likely to develop. Therefore, as suggested by Farley et al. (1970), the equatorial post-sunset electric field should play a dominant role on the variability of ESF.

During storms, the low-latitude electric fields can be significantly disturbed and two major sources of these perturbations are found in the magnetospheric and ionospheric disturbance dynamo: (1) the magnetospheric and high-latitude electric fields and (2) the disturbance dynamo electric field. Magnetospheric dynamo processes generate prompt electric field perturbations with time scales less than ~2 h. However, the ionospheric disturbance dynamo affects the low-latitude region several hours or longer (Fejer, 2002). Past studies have shown that the onset of magnetic activity in the late afternoon increases the occurrence of spread-F, amplitude scintillations of VHF and UHF beacons, and large-scale plasma depletions in the pre-midnight sector, while the onset of strong magnetic activity near the noon sector decreases the occurrence of these irregularities and depletions (e.g. Aarons, 1991; Abdu et al., 1995; Sahai et al., 1998).

For the storms presented previously, Table 1 outlines the scintillation occurrence. From the table and previous figures, we can clearly see that many indices (e.g. IMF Bz, Dst, dDst/dt) are suitable for investigations of scintillation, but the maximum dDst/dt determined time is nearly the same as the estimated penetration time, and it determined that local time plays a main role in the development of irregularities. When the maximum dDst/dt determined local time is close to post-sunset (18:00–22:00 LT), the prompt penetration eastward electric field will enhance the maximum prereversal eastward electric field, and therefore the upward drifts velocities. The prereversal velocity enhancements elevate the F layer to much higher altitudes, and then the scintillations or plasma bubbles will probably be observed as storms 1 and 2. Since the prompt penetration effects are short-lived, however, when the determined time is near the noon sector, after a few hours (near post-sunset), the westward disturbance dynamo effects control the dynamics of the low-latitude region. They reduce the prereversal eastward electric field and decrease the upward drift velocities, and so inhibit the generation of irregularities. As storm 3 presented, the spread-F phenomena or EPBs were observed at other longitude sectors, but at station Sanya, no scintillations or irregularities were detected. These results can be explained as due to the effects of eastward prompt penetration (trigger the scintillation occurrence) and westward ionospheric disturbance dynamo electric fields (inhibit the scintillation occurrence), respectively (Fejer and Scherliess, 1997; Scherliess and

Table 1
The storm sudden commencement time, the prompt penetration time, the maximum Dst negative excursion time and maximum dDst/dt time and determined local time for station Sanya (LT ≈ UT + 7), and longitude sectors where EPBs or ESF occur during the storm periods

Storm	SSC time (UT)	Penetration time (UT)	Maximum Dst (nT) and the time (UT and LT), LT ≈ UT + 7	Maximum dDst/dt (nT/h) and the time (UT and LT), LT ≈ UT + 7	Scintillation occurrence and the time (UT)	ESF or bubbles observed at longitude sectors and the time (UT)
8 May 2005	7 May, 19:16	~12:00	−127 nT, 18:00 UT 01:00 LT	−27 nT/h, 12:00 UT 19:00 LT	12:00–20:00, strong	
24 Aug 2005	06:13	~10:00	−216 nT, 11:00 UT 18:00 LT	−158 nT/h, 10:00 UT 17:00 LT	13:00–15:00, little	147°E, ~10:48
15 May 2005	02:39	~07:00	−263 nT, 08:00 UT 15:00 LT	−170 nT/h, 07:00 UT 14:00 LT	No	167°E, ~08:00–18:00 191°E, ~08:02
21 Jan 2005	17:11	~17:20	−99 nT, 21:00 UT 04:00 LT	63 nT/h, 18:00 UT 01:00 LT	No	29°E, ~18:54
30 May 2005	29 May, 09:52		−138 nT, 13:00 UT 20:00 LT	−27 nT/h, 08:00 UT 15:00 LT	No	172°E, ~09:18
12 Jun 2005	07:45	~18:00	−105 nT, 22:00 UT 05:00 LT	−34 nT/h, 19:00 UT 02:00 LT	No	19°E, 19:30
11 Sep 2005	01:14	~06:00	−123 nT, 10:00 UT 17:00 LT	−31 nT/h, 06:00 UT 13:00 LT	No	193°E, 07:48

Fejer, 1997). When the maximum dDst/dt determined local time is near the post-midnight sector, the irregularities develop related to the changing electric field direction. For the storms (21 January and 12 June, see Table 1), the strength of the added eastward electric field is probably not enough to change the electric field direction from westward to eastward, and does not trigger the post-midnight scintillation occurrence. When we categorized dDst/dt variations as the Aarons category (using maximum dDst/dt instead of maximum negative Dst), it indicates that the category 3 storms help to generate the irregularities associated with scintillations, category 2 storms did not trigger the scintillation and category 1 storms had more suitable conditions for the inhibition.

5. Conclusions

We have used GPS scintillation/TEC data to investigate the effects (trigger or inhibit/not trigger) of geomagnetic storms of the year 2005 on ionospheric scintillations at Sanya, the southmost station in the Chinese longitude region. Magnetometer data, Digisonde data (Chungli and Kwajalein) and topside plasma data were also used to help elucidate the possible mechanisms responsible for the effects. The main results can be summarized as follows.

The storms presented here with sharp increase in ΔH showed that prompt penetration occurs. Nearly the estimated penetration time, the maximum dDst/dt was observed. This supports the conclusion as Martinis et al. (2005) reported that the maximum dDst/dt determined time probably can be used as a proxy to determine the penetration time.

For storms 1, 2 and 3, strong, little and no scintillation activities were observed, respectively, at Sanya. For storms 1 and 2, they occurred at J month (May–August, the minimum scintillation occurrence season for Sanya). We think storms 1 and 2 trigger the scintillation occurrence, and storm 3 does not generate the irregularities observed at Sanya. But for storm 3, the EPBs or spread-F were observed at other longitude regions, where the dDst/dt determined local time is close to post-sunset. It signifies that storm 3 triggers the scintillation occurrence at other longitude sectors.

The cases listed in Table 1 indicate that the storm effects on scintillation depend on the maximum dDst/dt determined local time sector. When the determined local time is close to post-sunset, the enhanced eastward electric field sets the plasma into motion via the vertical $\mathbf{E} \times \mathbf{B}$ drift, which causes the Rayleigh–Taylor mode to become unstable, and leads to the development of plasma bubbles and spread-F irregularities producing scintillation. These can be explained as due to the combined effects of magnetosphere and ionosphere disturbance electric fields (Fejer–Scherliess model). By using maximum dDst/dt indices instead of maximum negative Dst indices, the storm effects on ionospheric scintillations in these events can be categorized as "Aarons criteria".

Statistical analysis of Kp and scintillation indices shows that most storms of the year have not triggered the scintillation occurrence at Sanya. This is because the maximum dDst/dt determined local time (for station Sanya) is near the noon (or post-midnight) sector for most storms of the year 2005, which inhibited (or did not trigger) the post-sunset (or post-midnight) scintillation occurrence.

Acknowledgments

This research was supported by the National Natural Science Foundation of China (40774091, 40574072, 40374054) and the KIP Pilot Project (KZCX3-SW-144) of the Chinese Academy of Sciences, and partly supported by the Chinese Arctic and Antarctic Administration (20070209). The authors thank the referees for their corrections and valuable suggestions to improve the paper, and acknowledge UT-Dallas for providing the DMSP data.

References

Aarons, J., 1982. Global morphology of ionospheric scintillations. Proceedings of the IEEE 70, 360–373.

Aarons, J., 1991. The role of the ring current in the generation or inhibition of equatorial F-layer irregularities during magnetic storms. Radio Science 26, 1131–1149.

Aarons, J., DasGupta, A., 1984. Equatorial scintillations during the major magnetic storm of April 1981. Radio Science 19, 731–739.

Abdu, M.A., Batista, I.S., Walker, G.O., Sobral, J.H.A., Trivedi, N.B., de Paula, E.R., 1995. Equatorial ionospheric electric fields during magnetospheric disturbances: local time/longitude dependencies from recent EITS campaigns. Journal of Atmospheric and Terrestrial Physics 57, 1065–1083.

Allen, J., Frank, L., Sauer, H., Reiff, P., 1989. Effects of the March, 1989 solar activity. EOS Transactions of the American Geophysical Union 70, 1479–1488.

Basu, S., Mackenzie, E., Basu, S., 1988. Ionospheric constraints on VHF/UHF communication links during solar maximum and minimum periods. Radio Science 23, 363–372.

Basu, S., Groves, K.M., Quinn, J.M., Doherty, P., 1999. A comparison of TEC fluctuations and scintillations at Ascension

Island. Journal of Atmospheric Terrestrial Physics 61, 1219–1226.

Basu, S., Basu, S., Valladares, C.E., Yeh, H.-C., Su, S.-Y., Mackenzie, E., Sultan, P.J., Aarons, J., Rich, F.J., Doherty, P., Groves, K.M., Bullett, T.W., 2001. Ionospheric effects of major magnetic storms during the international space weather period of September and October 1999: GPS observations, VHF/UHF scintillations, and in situ density structures at middle and equatorial latitudes. Journal of Geophysical Research 106 (A12), 30389–30414.

Biktash, L.Z., 2004. Role of the magnetospheric and ionospheric currents in the generation of the equatorial scintillations during geomagnetic storms. Annales Geophysicae 22, 3195–3202.

Chandra, H., Rastogi, R.G., 1974. Geomagnetic storm effects on ionospheric drifts and the equatorial ES over the magnetic equator. Indian Journal of Radio & Space Physics 3, 332–336.

Dabas, R.S., Lakshmi, D.R., Reddy, B.M., 1989. Effect of geomagnetic disturbances on VHF nighttime scintillation activity at equatorial and low latitudes. Radio Science 4, 563–573.

Farley, D.T., Balsley, B.B., Woodman, R.F., McClure, J.P., 1970. Equatorial spread F: implications of VHF radio observations. Journal of Geophysical Research 75, 7199–7216.

Fejer, B.G., 1996. Natural ionospheric plasma waves. In: Kohl, H., Ruster, R., Schelegel, K. (Eds.), Modern Ionospheric Science. Max-Planck Institute For Aeronomy, Lindau, Germany, pp. 217–273.

Fejer, B.G., 2002. Low latitude storm time ionospheric electrodynamics. Journal of Atmospheric and Solar Terrestrial Physics 64, 1401–1408.

Fejer, B.G., Kelley, M.C., 1980. Ionospheric irregularities. Reviews of Geophysics 18, 401–450.

Fejer, B.G., Scherliess, L., 1997. Empirical models of storm time equatorial zonal electric fields. Journal of Geophysical Research 102, 24047–24056.

Fejer, B.G., Scherliess, L., de Paula, E.R., 1999. Effects of the vertical plasma drift velocity on the generation and evolution of equatorial spread F. Journal of Geophysical Research 104 (A9), 19859–19869.

Huang, C.Y., Burke, W., Machuzak, J., Gentile, L., Sultan, P., 2002. Equatorial plasma bubbles observed by DMSP satellites during a full solar cycle: toward a global climatology. Journal of Geophysical Research 107 (12), 1434, doi:10.1029/2002JA009452.

Kelley, M.C., 1989. The Earth's Ionosphere: Plasma Physics and Electrodynamics. International Geophysics Series, 43. Academic Press, San Diego, CA.

Kelley, M.C., Maruyama, T., 1992. A diagnostic method for equatorial spread F, 2, the effect of magnetic activity. Journal of Geophysical Research 97, 1271–1277.

Li, G., Ning, B., Wan, W., Zhao, B., 2006. Observations of GPS ionospheric scintillations over Wuhan during geomagnetic storms. Annales Geophysicae 24, 1581–1590.

Ma, G., Maruyama, T., 2006. A super bubble detected by dense GPS network at east Asian longitudes. Geophysical Research Letters 33, L21103.

Martinis, C.R., Mendillo, M.J., Aarons, J., 2005. Toward a synthesis of equatorial spread F onset and suppression during geomagnetic storms. Journal of Geophysical Research 110.

Pi, X., Mannucci, A.J., Lindqwister, U.J., Ho, C.M., 1997. Monitoring of global ionospheric irregularities using the worldwide GPS network. Geophysical Research Letters 24 (18), 2283–2286.

Rich, F.J., Hairston, M., 1994. Large-scale convection patterns observed by DMSP. Journal of Geophysics Research 99 (A3), 3827–3844.

Sahai, Y., Fagundes, P.R., Bittencourt, J.A., Abdu, M.A., 1998. Occurrence of large scale equatorial F-region depletions during geo-magnetic disturbances. Journal of Atmospheric and Solar Terrestrial Physics 60, 1593–1604.

Scherliess, L., Fejer, B.G., 1997. Storm time dependence of equatorial disturbance dynamo zonal electric fields. Journal of Geophysical Research 102, 24037–24046.

Tsurutani, B.T., Gonzalez, W.D., Tang, F., Lee, Y.T., 1992. Great magnetic storms. Geophysical Research Letters 19, 73–76.

Van Dierendonck, A.J., Hua, Q., Klobuchar, J., 1993. Ionospheric scintillation monitoring using commercial single frequency C/A code receivers. In: Proceedings of ION GPS 93, Salt Lake City, UT, 22–24 September 1993, pp. 1333–1342.

Woodman, R.F., La Hoz, C., 1976. Radar observations of F region equatorial irregularities. Journal of Geophysical Research 81, 5447–5466.

Xu, J.S., Zhu, J., Cheng, G.H., 2006. GPS observations of ionospheric effects of the major storm of Nov. 7–10, 2005. Chinese Journal of Geophysics 49 (4), 950–956.

Xu, J.S., Zhu, J., Li, L., 2007. Effects of a major storm on GPS amplitude scintillations and phase fluctuations at Wuhan in China. Advances in Space Research 39, 1318–1324.